Tilted Fiber Bragg Grating photowritten in microstructured optical fiber for improved refractive index measurement

Minh-Châu Phan Huy, Guillaume Laffont, Véronique Dewynter, Pierre Ferdinand, Laurent Labonté, Dominique Pagnoux, Philippe Roy, Wilfried Blanc, Bernard Dussardier

Tilted Fiber Bragg Grating photowritten in Microstructured Optical Fiber for improved refractive index measurement

Minh Châu Phan Huy, Guillaume Laffont, Véronique Dewynter and Pierre Ferdinand

CEA LIST, Centre d'Etudes de Saclay, 91191 Gif-sur-Yvette cedex France
minhchau.phanhuy@gmail.com guillaume.laffont@cea.fr

Laurent Labonté, Dominique Pagnoux and Philippe Roy

Xlim – Département photonique, UMR-CNRS 6172, 123 Avenue Albert Thomas, 87060 Limoges cedex, France

Wilfried Blanc and Bernard Dussardier

LPMC / FOA, UMR-CNRS 6622, Université de Nice Sophia-Antipolis, Parc Valrose, 06108 Nice France

Abstract: We report what we believe to be the first Tilted short-period Fiber Bragg Grating photowritten in a microstructured optical fiber for refractive index measurement. We investigate the spectral sensitivity of Tilted Fiber Bragg Grating to refractive index liquid inserted into the holes of a multimode microstructured fiber. We measure the wavelength shift of the first four modes experimentally observed when calibrated oils are inserted into the fiber holes, and thus we determine the refractive index resolution for each of these modes. Moreover, a cross comparison between experimental and simulation results of a modal analysis is performed. Two simulation tools are used, respectively based on the localized functions method and on a finite element method. All results are in very good agreement.

OCIS codes: (050.2770) Gratings; (060.0060) Fiber optics and optical communications; (060.2280) Fiber design and fabrication; (060.2370) Fiber optic sensors; (230.3990) Microstructure devices

References and Links

1. N. G. R. Broderick, T. M. Monro, P. J. Bennet, and D. J. Richardson, "Non linearity in holey optical fibers: measurement and future opportunities," Opt. Lett. **24**, 1395-1397 (1999)
2. J. H. Lee, W. Belardi, T. M. Monro, and D. J. Richardson, "Holey fiber based nonlinear optical devices for telecommunications," Proc. 29th CLEO/QELS (Baltimore, June 2003)
3. P. Andrés, A. Ferrando, E. Silvestre, J. J. Miret, and M. V. Andrés, "Dispersion and polarization properties in photonic crystal fibers," Proc. 4th Int. Conf. on Transparent Optical Networks ICTON (2002)
4. A. Bjarklev, J. Broeng, S. Barkou, and K. Dridi, "Dispersion properties of photonic crystal fiber," 24th ECOC Conf. (Madrid, Sept. 1998)
5. W.J. Wadsworth, R. M. Percival, G. Bouwmans, J. C. Knight, and P. S. J. Russell, "High power air-clad photonic crystal fiber laser," Opt. Express **11**, 48-53 (2003)
6. D. Pagnoux *et al.*, "Microstructured fibers for sensing applications," invited paper Proc. 17th Int. Conf. on Optical Fibre Sensors OFS17 (Bruges, May 2005)
7. N. Groothoff, J. Canning, E. Buckley, K. Lyttikainen, and J. Zagari, "Bragg gratings in air-silica structured fibers," Opt. Lett. 28, 233-235 (2003)
8. G. Kakarantzas, A. Malki, S. Février, P. Roy, and D. Pagnoux, "Structural long period gratings in photonic crystal fibers," Opt. Lett. 27, 1013-1015 (2002)
9. G. Humbert, A. Malki, S. Février, P. Roy, and D. Pagnoux, "Electric arc-induced long-period gratings in Ge-free air-silica microstructured fibres," Electron. Lett. **39**, 349-350 (2003)
10. J. Canning, N. Groothoff, E. Buckley, T. Ryan, K. Lyttikainen, and J. Digweed, "All-fibre photonic crystal distributed Bragg reflector fibre laser," Opt. Express **11**, 1995-2000 (2003)
11. B.J. Eggleton, P. S. Westbrook, R. S. Windeler, S. Spalter, and T. A. Strasser, "Grating resonances in air-silica microstructured optical fibers," Opt. Lett. 24, 1460-1462 (1999)

12. G. Laffont and P. Ferdinand, "Tilted short-period fiber-Bragg-grating-induced coupling to cladding modes for accurate refractometry," Meas. Sci. Technol. **12**, 765-770 (July 2001)
13. G. Laffont and P. Ferdinand, "Mesure de la salinité et suivi de polymérisation d'une résine à l'aide d'un réfractomètre à réseau de Bragg à traits inclinés," Optix 2001, Marseille 26-28 Novembre
14. M. C. Phan Huy, G. Laffont , V. Dewynter-Marty, P. Ferdinand, P. Roy , J-M. Blondy, D. Pagnoux, W. Blanc, and B. Dussardier, "Fiber Bragg grating photowriting in microstructured optical fibers for sensing application based on refractive index measurement," Proc. 17th Int. Conf. on Optical Fibre Sensors OFS17 (Bruges, May 2005)
15. M. C. Phan Huy, G. Laffont, Y. Frignac, V. Dewynter-Marty, P. Ferdinand, P. Roy, J-M. Blondy, D. Pagnoux, W. Blanc and B. Dussardier, "Fibre Bragg Grating photowriting in microstructured optical fibres for refractive index measurement," Meas. Sci. Technol. **17**, pp 992-997 (2006)
16. P. S. Westbrook, B. J. Eggleton, R. S. Windeler, A. Hale, T. A. Strasser and G. L. Burdge, "Cladding-Mode Resonances in Hybrid Polymer–Silica Microstructured Optical Fiber Gratings," IEEE Photon. Technol. Lett. **12**, 495-497 (2000)
17. C. Kerbage, B. Eggleton, P. Westbrook and R. Windeler, "Experimental and scalar beam propagation analysis of an air-silica microstructure fiber," Opt. Express **7**, pp. 113-122 (2000)
18. R. Parmentier, M. C. Phan Huy, G. Laffont , V. Dewynter-Marty, P. Ferdinand, P. Roy , J-M. Blondy, D. Pagnoux, and B. Dussardier, "Cross comparison between theoretical and experimental modal field patterns in a doped-core microstructured fiber," Summer school on advanced glass-based nanophotonics POWAG 2004
19. D. Mogilevtsev, T. A. Birks, and P. S. J. Russel, "Group-velocity dispersion in photonic crystal fibers," Opt. Lett. **23**, 1662-1664 (1998)
20. T.M. Monro, D. J. Richardson, N. G. R. Broderick, and P. J. Bennett, "Holey optical fibers: an efficient modal model," IEEE J. Lightwave Technol. **17**, 1093-1101 (1999)
21. http://www.comsol.com/
22. L. Dong, G. Qi, M. Marro, V. Bhatia, L. L. Hepburn, M. Swan, A. Collier and D. L. Weidman, "Suppression of cladding mode coupling loss in fiber Bragg gratings," IEEE J. Lightwave Technol. **18**, 1583-1590 (2000)
23. G. Laffont, "Etude et développement de transducteurs et systèmes de mesure à réseaux de Bragg à traits inclinés photoinscrits dans des fibres optiques monomodes," Ph. D Thesis, Lille University (2001, n°2983).
24. G. Laffont, N. Roussel, L. Maurin, J. Boussoir, B. Clogenson, L. Auger, S. Magne and P. Ferdinand, "Wavelength tunable fiber ring laser for high-speed interrogation of fiber Bragg grating sensors," Proc. 17th Int. Conf. on Optical Fibre Sensors OFS17 (Bruges, May 2005)
25. S. D. Dyer, P. A. Williams, R. J. Espejo, J. D. Kofler and S. M. Etzel, "Fundamental limits in fiber Bragg grating peak wavelength measurements," *invited paper* Proc. 17th Int. Conf. on Optical Fibre Sensors OFS17 (Bruges, May 2005).

1. Introduction

Microstructured optical fibers (MOFs) are generally silica fibers with a solid core surrounded by a lattice of air holes running along the longitudinal axis. The core can be made of pure or doped silica. Because the refractive index of the core is higher than the highest effective index of the modes of the cladding, these fibers simply guide light by total internal reflection. Since a few years, such fibers are a great matter of concern for the optical fiber community due to their potential in several application fields (non-linear effects [1, 2], dispersion management [3, 4], high optical power transmission [5], and sensing [6]).

Different methods are described in the literature for Fiber Bragg Grating photowriting either in pure-silica or in doped core MOF. For pure-silica MOF, Fiber Bragg Gratings (FBGs) and Long-Period Gratings (LPGs) photowriting are respectively reported by Groothoff *et al.* [7] using a two-photon absorption process at 193 nm and by Kakarantzas *et al.* [8] using a CO_2 laser to periodically collapse the channels of the MOF by heat treatment. Humbert *et al.* [9] choose to use an electric arc technique to realize LPGs. For doped-core MOF, Canning *et al.* [10] use a two-photon absorption process at 193 nm to write gratings in Er^{3+}-doped aluminosilicate core photonic crystal fiber. In Ge-doped photosensitive fibers, Eggleton *et al.* [11] photowrite FBGs and LPGs using a phase mask setup with a frequency-doubled excimer-pumped dye laser. While different gratings (LPGs and FBGs) have been already photowritten and characterized, we report in this paper what seems to be the first study dealing with Tilted Fiber Bragg Grating (TFBG) photowriting in microstructured optical fibers for sensing applications.

TFBGs photowritten in standard single-mode fibers are used for refractometry amongst other applications. TFBGs are spectrally sensitive to the refractive index of the medium surrounding the fiber's cladding [12]. Laffont *et al.* [13] relate two experiments consisting of

measuring the salinity of aqueous solutions and on following a resin polymerization process for smart manufacturing of composite materials, *via* TFBGs photowritten in standard single-mode fiber. The interaction between the optical electromagnetic field and the medium inserted into the holes may be stronger in MOF than in classical fiber, the interaction strength depending on a careful choice of holes pattern (MOF design). Hence, contrary to standard single-mode fiber, even standard FBGs photowritten in MOF may be very sensitive to a medium inserted into its holes. Refractive index measurement based on FBG photowritten in MOF has already been described in a previous work [14, 15], whereas in [16] the authors exploit the thermo-optic effect to tune the resonant wavelength of a LPG. Looking at the refractive index of the substance inserted into the holes of a MOF incorporating a FBG [14, 15], the resolution has been established to be about 4×10^{-3} r.i.u (refractive index unit) in the range of the refractive index values for water ($n \sim 1.33$), while for a fluid which refractive index is close to 1.45 the refractive index resolution reaches 6.8×10^{-6} r.i.u. [14, 15].

In this paper, we present the manufacturing of a Ge-doped core six-hole fiber as well as TFBG photowriting in such a fiber. In order to carefully characterize this MOF, a modal analysis is performed and the experimental modal field patterns are compared to LFM-computed and FEM-computed results, in a similar approach than the one presented in [17]. Calibrated liquids (index oils) are then inserted into the fiber holes and TFBGs spectral sensitivity to refractive index is then determined and compared to the sensitivity of standard FBGs photowritten in the same fiber.

2. Microstructured fiber manufacturing and design

For MOF manufacturing, the first step consists of realizing a preform which is a stack of silica capillaries and rods (a few millimeters in diameter). The number and the general arrangement of the air holes of the preform will be preserved in the fiber drawn. For a Ge-doped core MOF, we substitute the central silica rod by a Ge-doped silica rod of equal diameter. The Ge-doped core is manufactured by MCVD process. In order to extract the Ge-doped rod from the MCVD preform, two successive machining steps are needed. So in the case of the six-hole fiber presented on Fig. 1, the MCVD preform is first reduced from 12 mm to 2 mm through mechanical machining and then further reduced down to 1 mm through a chemical attack (HF acid). To draw the fiber, a conventional drawing tower is used. The manufactured fiber can be described by a ring of six air holes ($d \sim 15$ µm and $\Lambda \sim 15.8$ µm), surrounding a non-circular and slightly decentred core of 11 µm in diameter (see Fig. 1). Such a fiber is multimode in the 1.5 µm spectral window. The multimode aspect of the fiber will be experimentally verified in section 4.2.

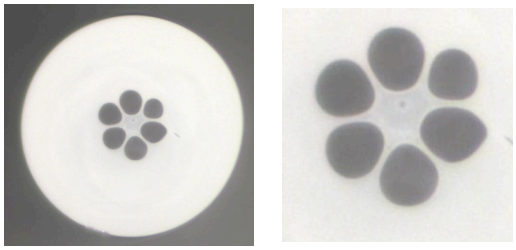

Fig. 1. Optical microscope image of the manufactured six-hole MOF.

3. Simulation tools

3.1. Localized functions method

A simulation tool based on a scalar version of the localized functions method (LFM) has been implemented [18]. In this method [19, 20] the modal electric field is decomposed on an orthonormal basis of Hermito-Gaussian functions. The interest of such functions is that they are localized in the vicinity of the fiber center and hence a suitable linear combination of them accurately describes guided modes. Our version of the simulation tool allows to integrate a

doped core into the index profile decomposition, so the index profile can be described by a sum of sinusoidal (describing the cladding) and Hermito-Gaussian (describing the doped core) functions. A scalar version of LFM implies that the influence of the state of polarisation of the guided light on the modal properties of the fiber cannot be studied, for instance in the case of a birefringent MOF fiber.

3.2. Finite element method

We have also used a wellknown and commercially available software called "Femlab" [21] that is based on the finite element method. This method consists of meshing in 2D a section of the optical waveguide (splitted into a number -often large- of discrete elements) to be analyzed and of solving the Maxwell equations in these points called "nodes". Femlab is used in our study to compare the FEM computed results and the LFM ones.

4. Tilted Fiber Bragg Grating photowriting

4.1. TFBG photowriting process

Fibers are previously hydrogen-loaded during one week at 150 bar and 25°C to increase the photosensitivity of the Ge-doped core and thus reduce the photowriting duration. Tilted FBGs are photowritten using a Lloyd mirror interferometer setup including a CW frequency-doubled argon laser emitting at 244 nm. To write TFBG, we need an angle different from $\pi/2$ between the Lloyd mirror and the fiber axis. In our setup, the fiber is held straight on between two clamps fixed on a rotary stage (see Fig. 2). In this way, we can easily and very accurately ($\pm 10^{-3}$ degree) adjust the required angle θ between the fiber axis and the interference fringes pattern.

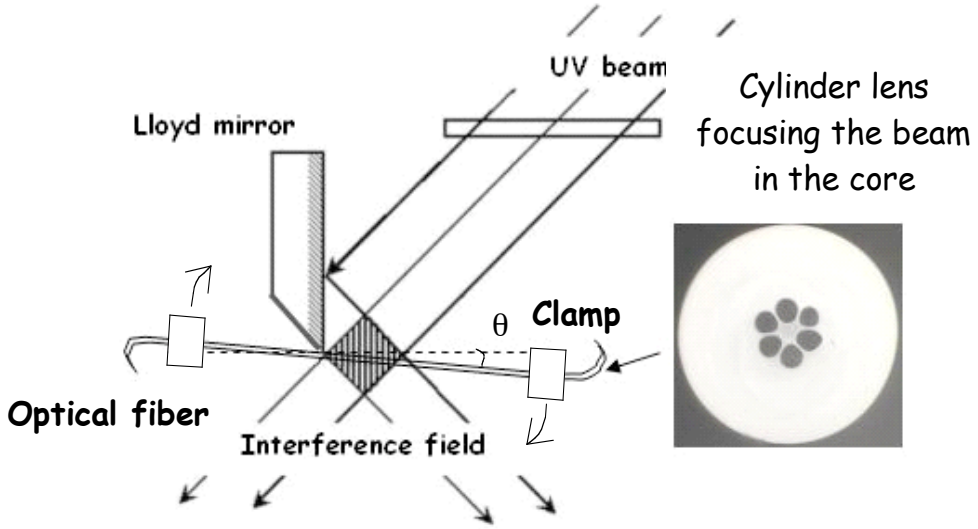

Fig. 2. Lloyd mirror interferometer setup used for TFBG photowriting.

On Fig. 3, we present transmission spectra of TFBGs photowritten in standard single-mode fiber. We notice the change in TFBGs spectral response when the tilt angle θ increases. For $\theta = 0°$, it is the coupling between the forward-propagating guided mode and the backward-propagating guided mode, corresponding to the so-called Bragg resonance, which is the most important. Resonances below 1538 nm correspond to the coupling between the fundamental mode (forward-propagating guided mode) and backward-propagating cladding modes (see Fig. 4). The coupling coefficient between the fundamental mode and a backward cladding mode is not null because the grating is spatially localized in the core: one way to decrease this coupling to cladding mode is precisely to extend the radius of the photosensitive region (hence

by using fiber with a photosensitive cladding) [22]. When the tilt angle increases, the coupling coefficient between the forward-propagating guided mode and the backward-propagating guided mode decreases. So, the Bragg resonance reflectivity decreases too. And the more the tilt angle θ increases, the more the coupling to cladding mode dominates and the coupling's optimum is obtained for modes' order higher and higher. On the transmission spectra, we notice that one resonance out of two presents a lower amplitude. These resonances with lower amplitude are the result of coupling between the fundamental guided mode and LP_{1n} cladding modes, the other resonances (with higher amplitude) are due to coupling between the fundamental guided mode and LP_{0n} cladding modes.

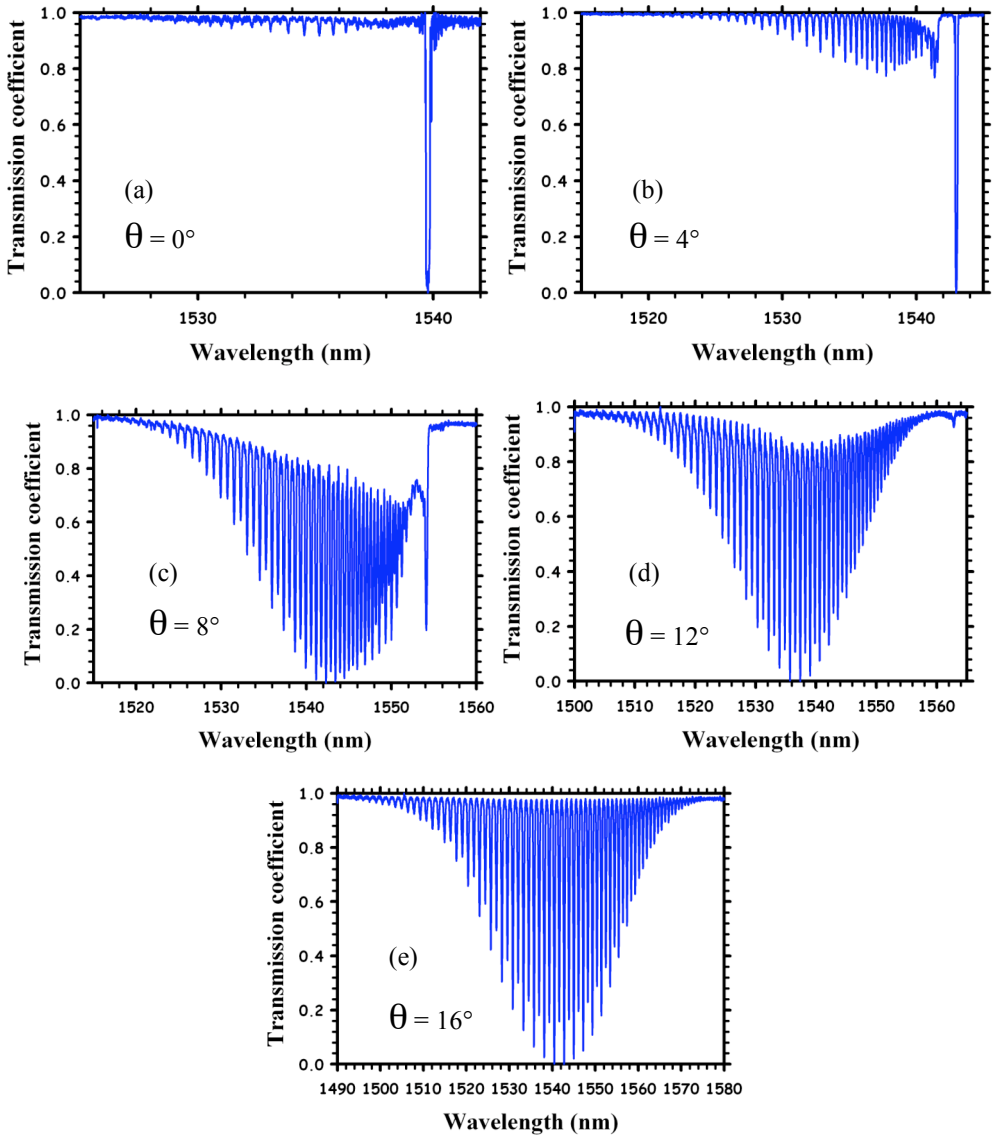

Fig. 3. Transmission spectra of (a) non-tilted, (b) 4°-tilted, (c) 8°-tilted, (d) 12°-tilted and (e) 16°-tilted FBGs photowritten in classical single-mode fiber with the Lloyd interferometer setup [23].

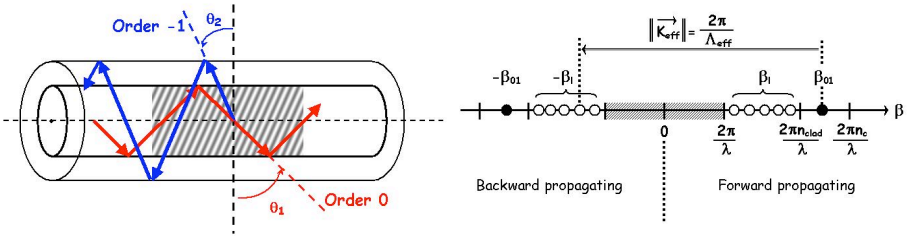

Fig. 4. Coupling between the fundamental mode (forward propagating guided mode) and backward cladding modes induced by TFBG [23]: on the right, coupling diagram showing the fundamental forward-propagating mode coupled to a backward-propagating cladding mode through the coupling vector (Λ_{eff} is the effective period of the grating, that is Λ – the fringe's period – divided by cos θ – the tilt angle).

In case of Fig. 3, fibers are placed in the air. Now, consider that the 16°-tilted TFBG, for instance, is surrounded by an external medium which refractive index (n_{ext}) is higher than 1.296 (up to this value the spectrum shape is almost the same for the 16°-tilted TFBG, only a small red shift of the resonances can be observed). When the external refractive index increases, we notice a gradual disappearance of the resonances composing the spectral response in transmission (see Fig. 5), from low wavelength resonances to high wavelength resonances. The forward guided mode is then not only coupled to the backward cladding modes but also to the continuum of radiation modes. When n_{ext} reaches the cladding refractive index value (n_{clad}), cladding modes are not any more guided, as the interface between the cladding and the external medium has disappeared. Only the coupling between the forward guided mode and the continuum of radiation modes is carried out. The TFBG spectral response in transmission is then a smooth envelope profile.

Based on this analysis, when n_{ext} varies, it is the global shape of the TFBG spectral response that is considered for sensing applications rather than the wavelength shift of a given spectral resonance [12, 23]. When n_{ext} increases, with $1.3 < n_{ext} < n_{clad}$, the area delimited by the upper and lower envelope curves decreases. So, once a calibration curve of area variations *versus* refractive index value has been established, such a grating can be used for sensing purposes [12, 13].

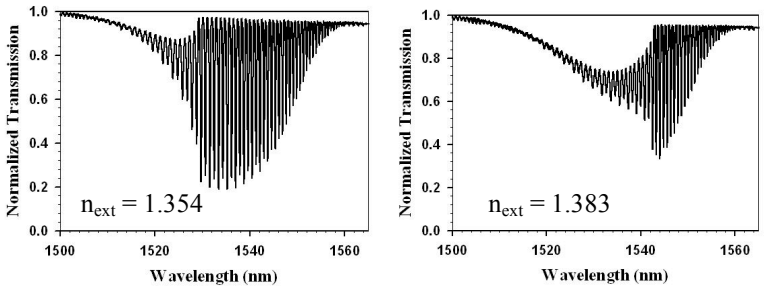

Fig. 5. Transmission spectrum of a 16°-tilted FBG photowritten in a standard singlemode fiber and for two distinct values of the surrounding refractive index [12].

4.2. Spectral response of a TFBG photowritten in MOF

On Fig. 6, we present spectral responses in transmission of TFBGs photowritten in the six-hole MOF presented in part 2 (see Fig. 1). For θ = 0°, we observe not only the Bragg resonance but also resonances to higher order modes. On the reflection spectrum, each mode is clearly characterized by a resonance peak, hence all of them may be considered as guided modes. Indeed the fiber was expected to be slightly multimode as already mentioned in section 2. When θ increases, more and more transmission dips are distinguishable on the spectrum, indicating that more and more modes are involved in the coupling process. As in the

case of TFBGs in conventional fiber, the higher the tilt angle, the higher the mode's order with the optimal coupling coefficient.

In order to characterize the propagation properties of such a photosensitive MOF fiber, and especially to obtain the field patterns of the guided modes, TFBGs are particularly useful: they can be used as a kind of "*mode selector*". Each spectral resonance corresponds to a guided (or a leaky) mode that may be imaged (depending on the optical losses). Once a given modal field pattern is acquired, together with the wavelength of the corresponding spectral resonance and hence the effective index of the mode, it is possible to establish accurate comparisons with modal computations (see section 5) performed using the simulation tools described in section 3: either the field patterns or the effective index may be compared.

The six-hole fiber is slightly birefringent due to the index profile's dissymmetry (holes diameters, pitch and core's shape). Moreover, the TFBGs photowriting's process also contributes to an extra birefringence effect (through radial asymmetry in UV light absorption and also due to the tilting of the grating's pitch *versus* the propagation axis). So when the state of polarization of the input light is modified, we can observe the splitting of any spectral resonance in two sub-resonances. This effect is particularly distinguishable for higher order modes.

As higher order modes are less and less optically confined in the core of the MOF, their evanescent field interacts more efficiently with any medium inserted into the holes. Hence, when a liquid is inserted into the fiber holes, all resonances experience a spectral displacement. The resonance's spectral shift is different from one mode to the other due to a more or less efficient evanescent field interaction. Hence, the sensitivity to the refractive index of the holes medium is increased when higher order modes' resonances are considered. In section 6, this potential gain in sensitivity is characterized for refractometry purposes.

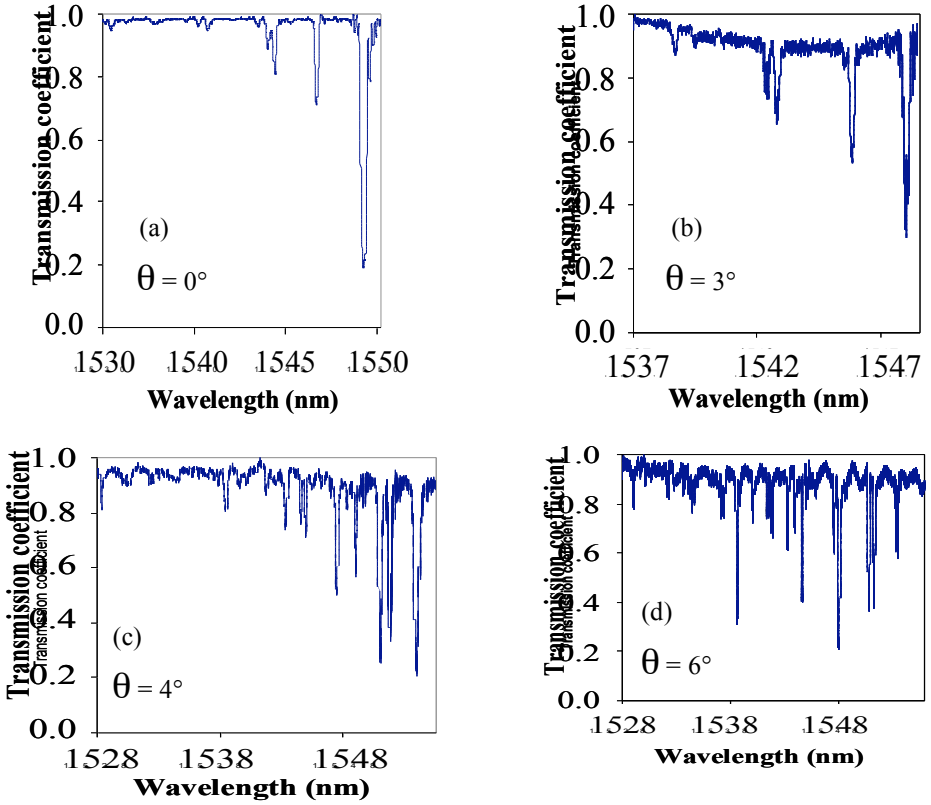

Fig. 6. Transmission spectrum of (a) non-tilted, (b) 3°-tilted, (c) 4°-tilted, (d) 6°-tilted FBG photowritten in the six-hole fiber.

5. Cross-comparison between theoretical and experimental modal field patterns

Our modal imaging setup used to characterize the modal field patterns of a multimode MOF takes benefit of a TFBG photowritten in the fiber to spectrally select the guided modes (and also leaky modes, depending on their optical losses). Using a spectrally tunable external-cavity diode laser (1 pm wavelength tuning resolution), we first acquire the transmission spectrum of the photowritten TFBG. Hence, we accurately determine each resonance wavelength. Then we successively tune the wavelength emitted by the laser to any the spectral resonances that we intend to image in reflection on a CCD near-infrared camera.

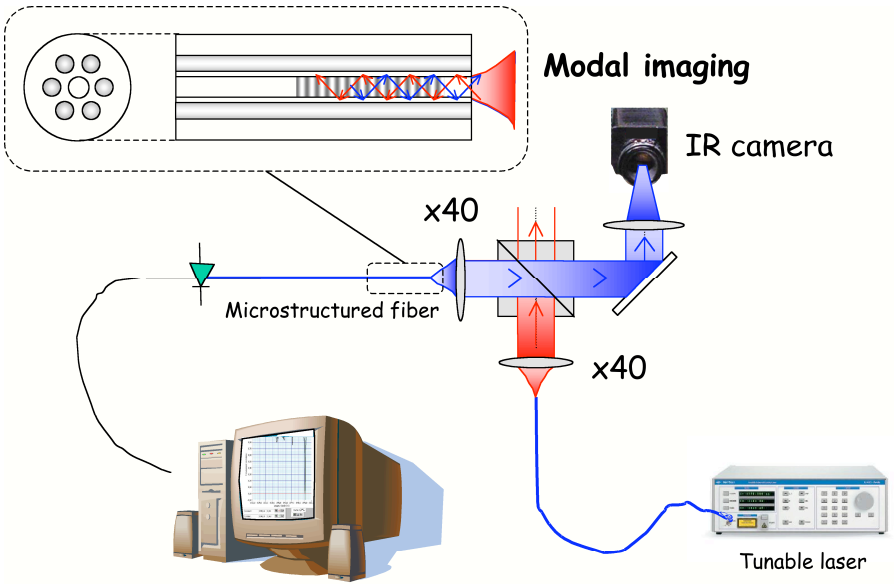

Fig. 7. Near-IR modal imaging setup.

The modal imaging setup (see Fig. 7) is composed of a tunable laser, two microscope objectives (x40), a beam splitter (50/50) and an InGaAs CCD camera (316 x 252 pixels, pixels size of 30 µm x 30 µm). All optical components are dedicated to work in the 1.5 µm spectral window. The tunable laser's light is injected in the core of the MOF: the injected optical power is optimized thanks to manually controlled translation stages of an optical fibers fusion splicer. Moreover, the MOF is cleaved as close as possible to the grating (less than 5 mm away from the grating), in order to increase the optical signal-to-noise ratio. Hence, even guided modes (or leaky modes) suffering from optical losses or with a low coupling coefficient may be observed.

Cross-section images of the six-hole fiber have been acquired using an optical microscope. We can determine the outline of the Ge-doped core thanks to its index contrast (see Fig. 1). This image is used as an entry parameter of the two simulation tools depicted in part 3 which outputs are the modal field patterns and effective indices that we can directly compare with those experimentally obtained.

As said in section 4.2, the fiber is birefringent, due to the fiber structure itself but also due to the tilted grating itself as well as to the photowriting process. The large refractive index contrast between the core and the cladding and the effect of the birefringence results in the splitting of the spectral resonances.

This splitting is visible only if the spectral variation between two subresonances, corresponding to the two polarisation states, is higher than the full width at half maximum (FWHM) of each resonance, which is about 200-300 pm. Moreover, this spectral variation increases with the mode's order. Contrarily to the LFM software which is only scalar, the full-vectorial modelling based on the FEM takes into account the state of polarisation of the input

light. However, by comparing the norms of the electric field for the two states of polarisation obtained by FEM, we do not notice any differences: the patterns' orientations and forms are similar [15]. Experimentally, we have imaged on the camera only one resonance corresponding to one of the two states of polarization and we have compared them to LFM and FEM simulation results. For FEM simulation results, we present only those corresponding to one state of polarization (see Fig. 8).

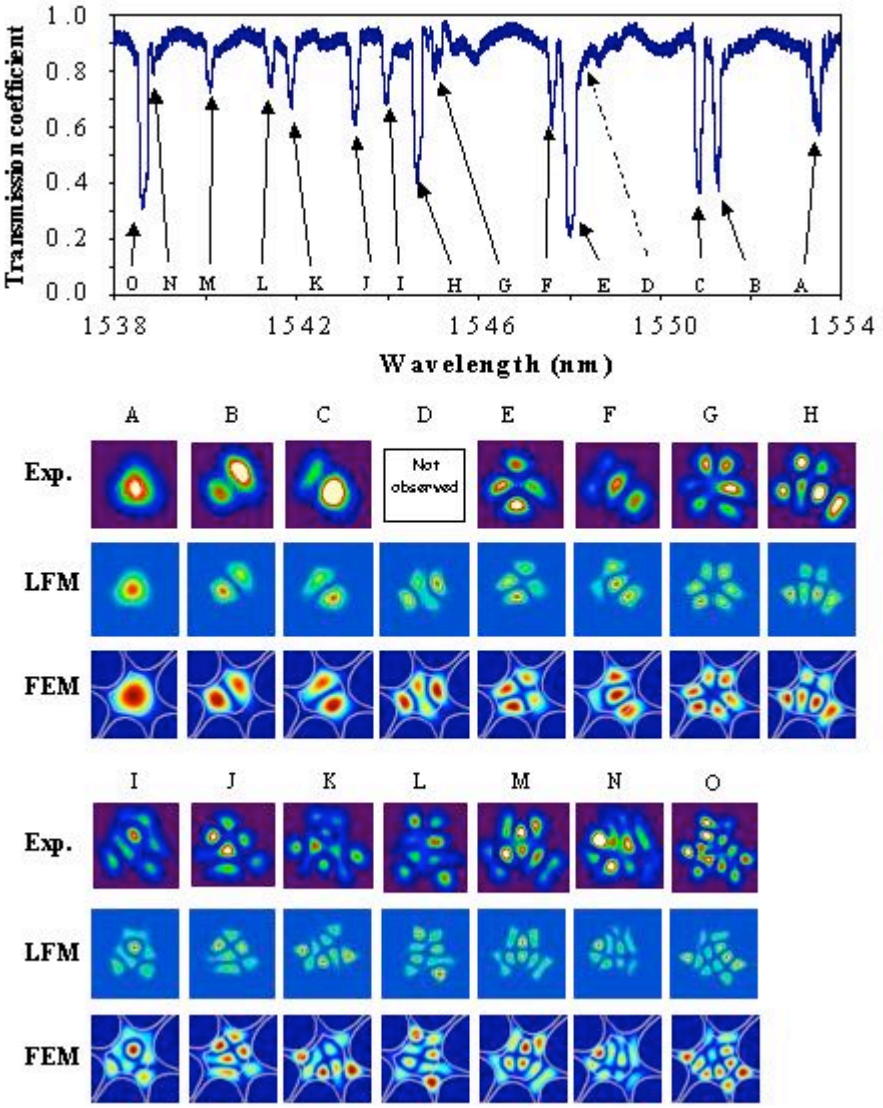

Fig. 8. Experimental TFBG transmission spectrum with corresponding experimental (top line), LFM-simulated (middle line) and FEM-simulated (bottom line, with commercial software Femlab) modal field pattern for the six-holes fiber

Fig. 8 shows the modal field patterns observed for the first fourteen spectral resonances of a 6°-TFBG together with those obtained through modelling (FEM and LFM methods). The modes observed have a rather complicated structure, particularly for high order ones. The mode geometry does not present any symmetry of revolution. The mode shape is strongly influenced by the fiber core's shape, which is not exactly circular for the six-hole MOF. As

can be seen, the modal patterns obtained by simulation (whatever the modelling method) correspond quite well to the experimental ones: the mode structure (number and intensity level of lobes) are in very good agreement. The three-lobe mode labeled "D" (see transmission spectrum at the top of Fig. 8) is not experimentally observed. To explain this, we infer that the opto-geometrical characteristics are not homogeneous along the fiber: holes diameter d and pitch Λ are not exactly the same at several fibers sections. Moreover, the optical micrography used for the simulation has been taken at a position different from that where the grating has been photowritten. It can be a source of error, which explains differences between simulation and experimental results. Even by changing the state of polarization of the input light, we cannot split any of the two E and F resonances (see the inset graph in Fig. 9(a)) to obtain finally three modes as obtained through modelling (D, E, F). Only the amplitude of the peak varies. But, when we analyze the spectral response of a TFBG photowritten in another section of the six-hole fiber, we visualize three resonances corresponding to the patterns of modes D, E and F (see the inserted graph in Fig. 9(b)). Hence this difference between experimental and modelling results may be mainly attributed to the non homogeneity of the MOF but also to the photowriting process itself: for instance, the fiber positioning between the clamps of the Lloyd interferometer setup influences the TFBG photowriting conditions. Moreover, we never know accurately how is positioned the fiber core facing the UV laser beam. Moreover the UV beam is not absorbed homogeneously by the fiber's core. Hence birefringence due to the TFBG photowriting process varies from one grating to another, even at the same tilt angle.

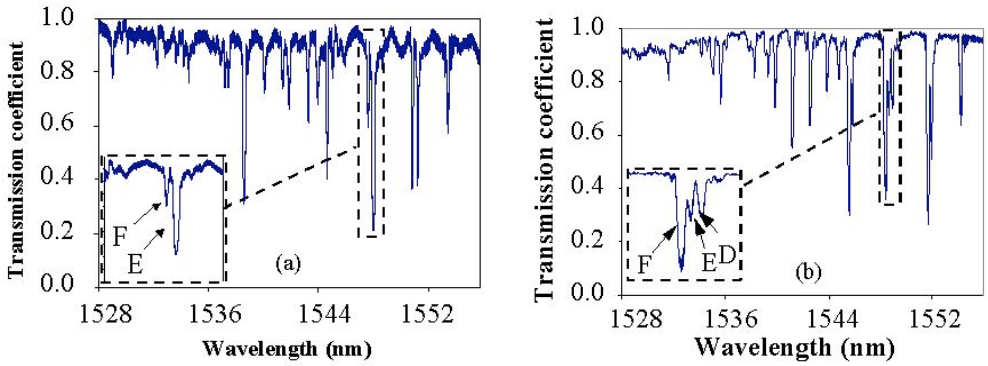

Fig. 9. Transmission spectrum of two 6°-tilted TFBGs photowritten in the core of two different sections of the six-holes fiber, revealing a) modes E and F or b) modes D, E, and F

6. TFBG spectral sensitivity to the refractive index of fluids inserted into the fiber channels

Contrarily to TFBGs photowritten in conventional single-mode fibers, TFBGs photowritten in the core of the six-hole fiber present fewer modes and the TFBG spectral response is different from one TFBG to another (even with the same tilt angle), as explained in section 5. Due to this variation in the TFBGs spectral responses, we cannot make use of the "area" approach, as introduced in section 3 in the case of TFBG in single-mode fiber, to determine the refractive index of the liquid inserted into the holes of the MOF. We rather choose to measure the spectral resonance shift *versus* the refractive index. Hence, we take benefit from the higher evanescent field interaction of the guided modes with the medium inserted into the channels.

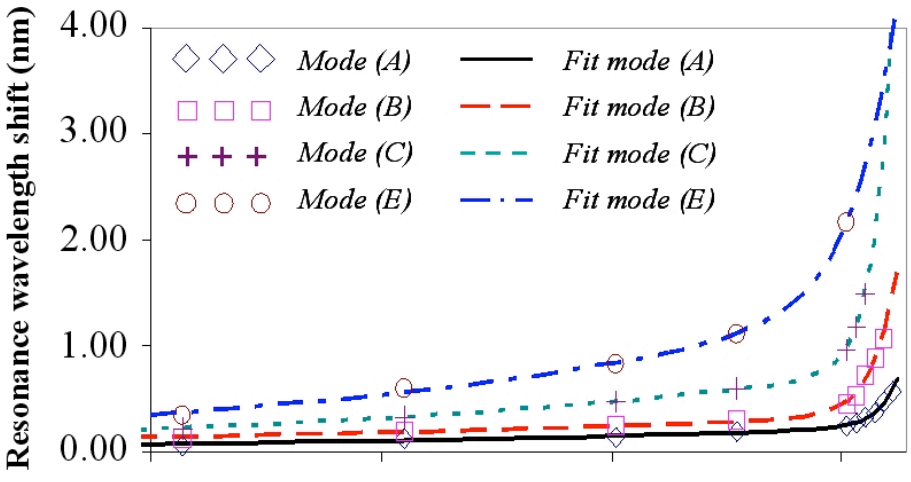

This experiment consists in introducing several calibrated refractive index liquids (Cargille's oils) into the holes of the MOF and to determine the consequences on the spectral resonances of a TFBG photowritten in its core. Refractive index n_L of liquids used in this experiment varies from 1.2960 to 1.4500 (@ 1550 nm / 25°C). These liquids are successively inserted into the fiber holes of a unique fiber section, without removing the previous one. The spectral resonances experience a red shift, when a given liquid reaches the TFBG (see Fig. 10). The insertion of any liquid modifies the interaction with the evanescent field of the guided mode and hence the effective index. The effective index of the guided modes increases together with the refractive index of the inserted liquid. We point out that the fourth mode (D) is not experimentally observed (see part 5). So, we follow experimentally the wavelength shift of the fundamental mode (A), the second mode (B), the third mode (C) and the fifth mode (E).

For a given mode, the evolution of the resonance wavelength with the refractive index is fitted by a sum of two exponential functions ($\lambda = a\ e^{bn_L} + c\ e^{dn_L}$). But, for mode (E), such a fit is not accurate enough. However, we notice that for refractive index close to 1.45, fitting curve of mode (E) intersects fitting curve of mode (C), which is not realistic. At this time, we do not have enough experimental data to accurately fit the evolution of the resonance wavelength of mode (E). This means that, for the mode (E), such a fit is not accurate enough. However such fitting curves can be used to determine the refractive index resolution at a given operating point on the wavelength *vs* refractive index curves. In Table 1, we report the refractive index resolution for several refractive index ranges. We assume that we have a 1 pm spectral resolution measurement setup, *i.e.* a typical value for FBG interrogation units [24, 25]. For a given mode, when the refractive index n_L approaches its effective index, the resonance wavelength shift increases, corresponding to a higher sensitivity and thus a better refractive index resolution. For the third mode (mode C), the refractive index resolution reaches 5.5×10^{-4} r.i.u. and 7.0×10^{-6} r.i.u. for a refractive index close to 1.300 and 1.444 respectively. In the same way, for a given refractive index, the wavelength shift is almost doubled from one mode to the following one. For instance, when the refractive index is equal to 1.301, the spectral shift is about 60 pm and 120 pm, respectively for mode (A) and mode (B) . So, the higher the mode order, the better the refractive index resolution. This is due to the fact that a higher order mode corresponds to a stronger evanescent field-external medium interaction (the mode is less confined within the fiber core). So, for a refractive index close to 1.30, the refractive index resolution is improved by a factor of 6, for the fifth mode (E) by comparison to the fundamental mode (A).

$\Delta\lambda$ = 1 pm	Refractive index resolution			
Refractive index	mode A	mode B	mode C	mode E
1.301	1.8×10^{-3}	1.2×10^{-3}	5.5×10^{-4}	3.0×10^{-4}
1.330	1.4×10^{-3}	1.0×10^{-3}	4.3×10^{-4}	2.3×10^{-4}
1.402	8.3×10^{-4}	6.4×10^{-4}	2.4×10^{-4}	–
1.422	6.7×10^{-4}	4.1×10^{-4}	1.8×10^{-4}	–
1.441	1.0×10^{-4}	3.1×10^{-5}	1.4×10^{-5}	–
1.444	5.6×10^{-5}	1.8×10^{-5}	7.0×10^{-6}	–
1.450	1.67×10^{-5}	6.3×10^{-6}	–	–

Table 1. Refractive index resolution of the first four modes (based on a 1 pm spectral resolution, [24]).

7. Conclusion

Tilted Fiber Bragg Gratings have been photowritten in the Ge-doped core of a six-hole microstructured optical fiber and have been characterized. TFBGs are useful in order to optimize the interaction between the fundamental guided mode and backward high order modes, and also to act as mode selectors. This allows to obtain the modal field patterns by near field imaging. The modal imaging experiment results show a good agreement with simulation ones, as the first fifteen fiber modes experimentally observed are also retrieved by the modelling. Then, the refractive index resolution of the first four modes experimentally observed is determined. The refractive index resolution value decreases with the increase of the mode order and with liquid refractive index value. Comparing to a FBG photowritten in the core of a six-hole fiber, refractive index resolution measured is improved by a factor of 17 (considering the fifth mode - labeled E - and for $n_L \sim 1.33$). So, depending on the refractive index range to analyze, it is possible to consider one mode or another to improve refractive index measurement. Hence this study highlights the metrological advantages of TFBGs in order to take benefit of the greater refractive index sensitivity of high order cladding modes. Refractive index sensitivity can also be improved by optimizing the MOF design to increase the interaction between the evanescent field and the medium inserted into the holes. In the future, the realisation of chemically selective refractometers combining functionalized microstructured fibers with an optimized holes pattern and appropriate Fiber Bragg Gratings transducers will be considered.

Acknowledgements

This research is co-funded by the French Ministry of Research – ACI Nouvelles Méthodologies Analytiques et Capteurs 2003 and by the INRS (*Institut National de Recherche et de Sécurité*).